INTERNATIONAL JOURNAL FOR NUMERICAL METHODS IN FLUIDS
Int. J. Numer. Meth. Fluids 2000; **33**: 1041–1073

Wind-driven currents in a sea with a variable eddy viscosity calculated via a Sinc–Galerkin technique

D. F. Winter[a], Kenneth L. Bowers[b,*] and John Lund[b]

[a] *Department of Physics, University of Redlands, Redlands, CA, U.S.A.*
[b] *Department of Mathematical Sciences, Montana State University, Bozeman, MT, U.S.A.*

SUMMARY

The Sinc–Galerkin method is presented as a new and potentially useful extension of the spectral method in numerical oceanography. To describe and illustrate the technique, a Sinc–Galerkin procedure is used to infer the sensitivity of wind-driven sub-surface currents in coastal regions and semi-enclosed seas when the vertical eddy viscosity coefficient is represented as a continuously differentiable function of depth. Problems with exact solutions are used to explore the accuracy and exponential convergence of expansions using composite translated sinc functions as a basis set. To illustrate the essential idea, we describe applications of the Sinc–Galerkin technique to modifications of the Ekman wind-drift current problem. Copyright © 2000 John Wiley & Sons, Ltd.

KEY WORDS: Sinc–Galerkin technique; sea currents; variable eddy viscosity

1. INTRODUCTION

Over the past several decades, extensive efforts have been made to develop numerical models of tide- and wind-driven currents and surface elevations in open and semi-enclosed seas. The earliest models of wind-driven current systems were one-dimensional in the vertical direction, inspired by the original work of Ekman [1]. A historical account of creative work on current patterns in open seas during the first half of this century is described in the classic reference by Defant [2]. Models developed during the 1950s were typically two-dimensional in the horizontal and either integrated over depth or consisted of layers in the vertical direction.

More than 25 years ago Heaps [3] proposed an eigenfunction expansion of horizontal currents in the vertical direction to convert the three-dimensional hydrodynamic equations to a two-dimensional system in the horizontal. Heaps assumed the vertical eddy viscosity coefficient to be constant with depth and employed a linear stress condition at the seabed [3,4] as well as a no-slip condition [5], both of which lead to sines and cosines as basis functions for

* Correspondence to: Department of Mathematical Sciences, Montana State University, PO Box 172400, Bozeman, MT 59717-2400, U.S.A.

Received 6 February 1997
Revised 6 October 1999

his expansions. More recently, extensions of Heap's approach, now referred to as the spectral method, coupled with a Galerkin approach have been developed. In a series of papers, the implications and utility of several basis function sets have been examined, including fourth-order B-splines by Davies [6] and Chebyshev and Legendre polynomials by Davies and Owen [7]. A strong motivation for examining various basis functions is the improvement of the resolution in the region where the magnitude of velocity shear is greatest—usually near the surface. These efforts encompassed three different seabed boundary conditions—linear and quadratic bottom stress and zero velocity—as well as vertical eddy viscosity representations by piecewise continuous straight lines. A survey of this work with an extensive list of references has been presented by Davies [8].

We suggest that for large near-surface velocity shears, it may be advantageous to choose sinc functions as basis functions. Sinc functions are particularly well suited for oceanographic problems with boundary layers since they naturally give most weight to the solution in such regions. Moreover, the properties of sinc functions allow for especially accurate evaluations of the integrals that arise from an application of the Galerkin method. An additional benefit of the method is that program codes are relatively short and are easily modified for different cases.

Recently, sinc function methods have been developed to the point where depth- and time-dependent hydrodynamic models could be considered and solved by the Sinc–Galerkin approach [9–12]. This sinc function procedure may eventually prove to be a useful complement to finite element and time stepping methods currently used in comprehensive models of coastal seas. Since a primary objective of this paper is to introduce an approximation technique that may be unfamiliar to the reader, the developments herein are limited to Sinc–Galerkin solutions of steady state wind-drift problems, with depth-dependent vertical eddy viscosity.

Following a convenient non-dimensionalization of the governing equations in Section 2, the Sinc–Galerkin solution method is described in some detail in Section 3. Appendix A is included to amplify the details of sinc function techniques. Section 4 presents an assessment of accuracy and computational speed of the method for the constant eddy viscosity case. In Section 5, practical examples of the Sinc–Galerkin approach are given, which illustrate the influence of depth-dependent eddy viscosity on wind-driven sub-surface current distributions. Again accuracy and computational speed are reported. Finally, in Section 6 we highlight the appropriateness of this technique for oceanographic computations. Appendix B is included to describe the alterations necessary to apply this method to the model with quadratic stress at the seabed.

2. GOVERNING EQUATIONS

Since the conservation equations of momentum, mass, and heat and salt (if appropriate) do not constitute a closed system, the prescription of turbulent eddy coefficients represents an empirical closure of the governing equations. This closure is referred to as a 'specified eddy viscosity model'. As has been pointed out in Reference [13], despite its simplicity this type of model 'has been used quite successfully in a number of shallow sea simulations' and although

such 'models do not contain all the sophistication of the turbulence closure models and may therefore be quite limited in the accuracy of the solution, they do give significant insight into the role of eddy viscosity and how its magnitude and variation influences the flow field'. In this spirit, we suppose that field measurements, or output from comprehensive models applied to similar waters, suggest representations of the principal feature of the effective vertical eddy viscosity as a continuously differentiable function of depth.

We use a right-handed co-ordinate system with the vertical co-ordinate z^* directed positive downward from the free surface, and with x^* and y^* directed northward and eastward respectively. A plane at $z^* = D_0$ corresponds to the impermeable boundary at the seabed. For the purpose of illustrating the Sinc–Galerkin approximation, we employ several of the simplifying assumptions invoked in one-dimensional wind-drift studies—the ocean depth, D_0, and mass density, ρ, are assumed constant, and the effects of tides, inertial terms, free surface slope, and variations in atmospheric pressure are neglected. Currents are driven by a tangential surface ($z^* = 0$) wind stress of magnitude τ_w represented as $\boldsymbol{\tau}(0) = \tau_w(\cos(\chi)\hat{\boldsymbol{x}}^* + \sin(\chi)\hat{\boldsymbol{y}}^*)$, with χ being the angle between the positive x^* axis and the wind direction. Here $\hat{\boldsymbol{x}}^*$ and $\hat{\boldsymbol{y}}^*$ represent unit vectors in the directions of the positive x^* axis and the positive y^* axis respectively. In a specified eddy viscosity model, internal frictional stresses are parameterized as $\boldsymbol{\tau}(z^*) = -\rho A_v^*(z^*)\, \mathrm{d}\boldsymbol{q}^*/\mathrm{d}z^*$, where the effective vertical eddy viscosity coefficient $A_v^*(z^*)$ is a prescribed continuously differentiable function of $z^* \in (0, D_0)$ and ρ is the ocean mass density. Here $\boldsymbol{q}^*(z^*) = U^*(z^*)\hat{\boldsymbol{x}}^* + V^*(z^*)\hat{\boldsymbol{y}}^*$ represents the horizontal wind-drift current that, in a linear theory, is the difference between the total velocity and the geostrophic current.

Under the present assumptions, the conservation of linear momentum equations express a balance between the Coriolis force and the internal friction associated with turbulence. The wind-drift current $\boldsymbol{q}^*$ is determined by solving the boundary value problem

$$\frac{\mathrm{d}}{\mathrm{d}z^*}\left[A_v^*(z^*)\frac{\mathrm{d}\boldsymbol{q}^*}{\mathrm{d}z^*}\right] = -f\hat{\boldsymbol{z}}^* \times \boldsymbol{q}^*, \quad 0 < z^* < D_0 \tag{2.1}$$

where the stress condition at the sea surface $z^* = 0$ is the tangential surface wind stress

$$-\rho A_v^*(0)\frac{\mathrm{d}\boldsymbol{q}^*(0)}{\mathrm{d}z^*} = \tau_w(\cos(\chi)\hat{\boldsymbol{x}}^* + \sin(\chi)\hat{\boldsymbol{y}}^*) \tag{2.2}$$

while at the seabed, $z^* = D_0$, the frictional stress is linearly proportional to the current, hence

$$-\rho A_v^*(D_0)\frac{\mathrm{d}\boldsymbol{q}^*(D_0)}{\mathrm{d}z^*} = k_f \rho \boldsymbol{q}^*(D_0) \tag{2.3}$$

Here $f \equiv 2\Omega \sin\theta$ is the Coriolis parameter at latitude θ, where $\Omega = 7.29 \times 10^{-5}$ rad s^{-1} is the angular speed of rotation of the earth and k_f is the linear slip bottom stress coefficient. The alternative zero-velocity (no-slip) condition, $\boldsymbol{q}^*(D_0) = 0$, can be handled by a minor modification of the subsequent developments, while the extension to a quadratic bottom stress at the seabed is briefly described in Appendix B.

If vertical eddy momentum exchange were constant, an Ekman depth and a characteristic velocity could be introduced in the standard way. For the present problem, one begins with a measure of near-surface turbulent eddy viscosity, $A_0 \equiv A_v^*(0)$. To non-dimensionalize the model equations, define a nominal 'upper-layer' Ekman depth by $D_E \equiv \sqrt{2A_0/|f|}$. Also, define a current speed in units of $U_0 = \tau_w D_E/(\rho A_0) = \sqrt{2}\tau_w/(\rho\sqrt{A_0|f|})$ (U_0 is the natural velocity scale in an infinitely deep sea with uniform eddy viscosity in the steady state). A non-dimensional form of the equations of motion can be expressed with the introduction of the non-dimensional variables

$$z \equiv \frac{z^*}{D_0}, \qquad A_v(z) \equiv \frac{A_v^*(z^*)}{A_v^*(0)}, \qquad \boldsymbol{q}(z) \equiv \frac{\boldsymbol{q}^*(z^*)}{U_0} \equiv U(z)\hat{\boldsymbol{x}} + V(z)\hat{\boldsymbol{y}} \tag{2.4}$$

together with two non-dimensional constants (a depth ratio κ and a bottom friction parameter σ) given by

$$\kappa \equiv \frac{D_0}{D_E} = D_0\sqrt{\frac{|f|}{2A_0}}, \qquad \sigma \equiv \frac{A_0 A_v(1)}{k_f D_0} = \frac{A_v^*(D_0)}{k_f D_0} \tag{2.5}$$

With these two definitions, the differential equations governing the velocity (in the Northern Hemisphere) can be written in component form as

$$-\frac{\mathrm{d}}{\mathrm{d}z}\left(A_v(z)\frac{\mathrm{d}U}{\mathrm{d}z}\right) = -2\kappa^2 V, \quad 0 < z < 1$$

and

$$-\frac{\mathrm{d}}{\mathrm{d}z}\left(A_v(z)\frac{\mathrm{d}V}{\mathrm{d}z}\right) = 2\kappa^2 U, \quad 0 < z < 1$$

subject to the surface boundary conditions

$$\frac{\mathrm{d}U(0)}{\mathrm{d}z} = -\kappa\cos(\chi), \qquad \frac{\mathrm{d}V(0)}{\mathrm{d}z} = -\kappa\sin(\chi)$$

At the seabed, the condition to be satisfied is linear stress

$$U(1) + \sigma\frac{\mathrm{d}U(1)}{\mathrm{d}z} = 0, \qquad V(1) + \sigma\frac{\mathrm{d}V(1)}{\mathrm{d}z} = 0 \tag{2.6}$$

In this formulation, the alternative no-slip condition can then be accomplished by setting $\sigma = 0$ in Equation (2.6). Appendix B discusses the quadratic bottom stress condition.

The linear transformations

$$U(z) = u(z) + \kappa(1 + \sigma - z)\cos(\chi), \qquad V(z) = v(z) + \kappa(1 + \sigma - z)\sin(\chi) \tag{2.7}$$

define the 'reduced velocity' components $u(z)$ and $v(z)$ satisfying

$$-\frac{\mathrm{d}}{\mathrm{d}z}\left(A_{\mathrm{v}}(z)\frac{\mathrm{d}u}{\mathrm{d}z}\right) + \kappa\cos(\chi)A'_{\mathrm{v}}(z) = -2\kappa^2 v - 2\kappa^3(1 + \sigma - z)\sin(\chi), \quad 0 < z < 1 \tag{2.8}$$

and

$$-\frac{\mathrm{d}}{\mathrm{d}z}\left(A_{\mathrm{v}}(z)\frac{\mathrm{d}v}{\mathrm{d}z}\right) + \kappa\sin(\chi)A'_{\mathrm{v}}(z) = 2\kappa^2 u + 2\kappa^3(1 + \sigma - z)\cos(\chi), \quad 0 < z < 1 \tag{2.9}$$

subject to the surface boundary conditions

$$\frac{\mathrm{d}u(0)}{\mathrm{d}z} = 0, \qquad \frac{\mathrm{d}v(0)}{\mathrm{d}z} = 0 \tag{2.10}$$

and the seabed boundary conditions

$$u(1) + \sigma\frac{\mathrm{d}u(1)}{\mathrm{d}z} = 0, \qquad v(1) + \sigma\frac{\mathrm{d}v(1)}{\mathrm{d}z} = 0 \tag{2.11}$$

For the purpose of clarifying the exposition of the Sinc–Galerkin technique, multiply Equation (2.9) by the imaginary unit i, add the result to Equation (2.8), and define a complex velocity $w(z) = u(z) + \mathrm{i}v(z)$. If one defines

$$Lw(z) \equiv -\frac{\mathrm{d}}{\mathrm{d}z}\left(A_{\mathrm{v}}(z)\frac{\mathrm{d}w}{\mathrm{d}z}\right) \tag{2.12}$$

the problem is now given by the system

$$Lw(z) - \mathrm{i}2\kappa^2 w(z) = F(z), \quad 0 < z < 1 \tag{2.13}$$

where

$$F(z) \equiv (-\kappa A'_{\mathrm{v}}(z) + \mathrm{i}2\kappa^3(1 + \sigma - z))\,\mathrm{e}^{\mathrm{i}\chi} \tag{2.14}$$

Repeating this procedure with Equation (2.10), the surface condition is

$$w'(0) = 0 \tag{2.15}$$

and with Equation (2.11), the seabed condition becomes

$$w(1) + \sigma w'(1) = 0 \tag{2.16}$$

3. SINC–GALERKIN SOLUTION OF THE STEADY STATE PROBLEM

The Sinc–Galerkin procedure for the problem in (2.13)–(2.16) begins by selecting composite sinc functions appropriate to the interval (0, 1) as the basis functions for the expansion of approximate solutions for the current components $w(x)$. Definitions, notation, and properties of sinc functions and composite sinc functions relevant to the discussion are recorded in Appendix A. This appendix also defines infinite sinc function expansions and presents error bounds on expansions that are truncated, such as those appearing in this treatment. With the introduction of a mapping function $\phi(z) = \ln(z/(1-z))$, the appropriate composite sinc functions, $S(k, h) \circ \phi(z)$, over the interval $z \in (0, 1)$ are defined as

$$S(k, h) \circ \phi(z) \equiv \operatorname{sinc}\left(\frac{\phi(z) - kh}{h}\right) \equiv \begin{cases} \dfrac{\sin[(\pi/h)(\phi(z) - kh)]}{(\pi/h)[\phi(z) - kh]}, & \phi(z) \neq kh \\ 1, & \phi(z) = kh \end{cases}$$

for $k = -N,\ -N+1, \ldots, N-1,\ N$.

When the boundary conditions are other than Dirichlet (the natural end conditions), alternative representations of the solution are provided in the immediate neighborhood of the end-points, since the sinc functions tend to zero and their derivatives become undefined as z approaches 0 or 1. The modification is accomplished by adding, to the sinc function expansion, third-order Hermite polynomials that correctly interpolate the unknown function and its derivatives at $z = 0$ and 1. The four cubic Hermite polynomials used to interpolate the solution at the boundaries in the case of mixed conditions at 0 and 1 are

$$h_0(z) = (2z+1)(1-z)^2, \qquad h_1(z) = z(1-z)^2, \qquad h_2(z) = (3-2z)z^2,$$

$$h_3(z) = (z-1)z^2 \tag{3.1}$$

By design, these functions are such that $h_0(0) = h_1'(0) = h_2(1) = h_3'(1) = 1$, and $h_0'(0) = h_0(1) = h_0'(1) = h_1(0) = h_1(1) = h_1'(1) = h_2(0) = h_2'(0) = h_2'(1) = h_3(0) = h_3'(0) = h_3(1) = 0$.

The approximate solution for $w(z)$, subject to the mixed conditions (2.15) and (2.16), is represented by the expansion

$$w_a(z) = c_{-N-1}B_0(z) + \sum_{k=-N}^{N} c_k \frac{S(k, h) \circ \phi(z)}{\phi'(z)} + c_{N+1}B_1(z) \tag{3.2}$$

where the expansion weight function, $1/\phi'(z) = z(1-z)$, has been introduced. The boundary polynomials $B_0(z)$ and $B_1(z)$, which interpolate the unknown function and its derivatives at $z = 0$ and 1, are easily assembled from Equation (3.1), using the definition of σ in (2.5), to give

$$B_0(z) = (2z+1)(1-z)^2, \qquad B_1(z) = (1-\gamma z)z^2 \tag{3.3}$$

where

$$\gamma \equiv \frac{1+2\sigma}{1+3\sigma}$$

It remains to determine the $m = 2N+3$ coefficients in the expansion $w_a(z)$ of (3.2), which approximate $w(z)$. The strategy for carrying out this task is outlined below as a five-step procedure, which yields a straightforward linear matrix equation for the unknown coefficients in the sinc function expansion.

Appendix A provides basic supplementary material concerning sinc functions and their properties. The Sinc–Galerkin approach to solving ordinary differential equations is summarized therein, together with theorems and results that are exceedingly useful during the procedure. Works by Lund and Bowers [10] and Stenger [11,12] may be consulted for additional mathematical details of sinc function theory, as well as references to other published work. In the discussion below we describe the main features of the Sinc–Galerkin procedure in the context of the problem at hand, providing intermediate results for the more complicated manipulations.

Step 1

Rewrite the governing differential equation (2.13) in the form

$$Lw_a(z) - i2\kappa^2 w_a(z) - F(z) = 0, \quad 0 < z < 1 \tag{3.4}$$

where

$$w_a(z) = w_h(z) + w_b(z) \tag{3.5}$$

Here

$$w_h(z) = \sum_{k=-N}^{N} c_k \frac{S(k,h)\circ\phi(z)}{\phi'(z)} \tag{3.6}$$

refers to the contribution to $w_a(z)$ associated with the homogeneous Dirichlet problem in the sinc expansion in Equation (3.2) and the subscript b indicates the boundary interpolations so that

$$w_b(z) = c_{-N-1}B_0(z) + c_{N+1}B_1(z) \tag{3.7}$$

Orthogonalize the residual with respect to the set of composite sinc functions $S(j,h)\circ\phi(z)\omega(z)$, with inner product weight $\omega(z)$, for $j = -N-1, -N, \ldots, N, N+1$. Now express the orthogonalized residual of Equation (3.4) as

$$\int_0^1 Lw_h(z)[S(j,h)\circ\phi(z)\omega(z)]\,dz + \int_0^1 [Lw_b(z) - i2\kappa^2 w_a(z) - F(z)][S(j,h)\circ\phi(z)\omega(z)]\,dz = 0 \tag{3.8}$$

The rationale for this maneuver is that only the integral involving $Lw_h(z)$ requires special treatment; the remaining integral can be accurately estimated using the special case of the sinc trapezoidal quadrature rule of (A.11) in Appendix A.

Step 2

Denote the first integral in Equation (3.8) by J, and approximate it by first integrating by parts twice to transfer derivatives from $w_h(z)$ to $S(j,h)\circ\phi(z)\omega(z)$. During this process, some clarity is achieved if $S(j,h)\circ\phi(z)$ is abbreviated to $S_j(z)$. Following two integrations by parts, J becomes

$$J=\left[-(S_j\omega A_v\omega_h')(z)+\left(S_j\omega'+\frac{dS_j}{d\phi}\phi'\omega\right)(z)A_v(z)w_h(z)\right]_0^1-\int_0^1[A_v(z)(S_j(z)\omega(z))']'w_h(z)\,dz \tag{3.9}$$

With regard to the first end-point contribution, from physical considerations it is reasonable to assume that the reduced velocity shear $w'(z)$ remains bounded as z approaches 0 and 1. Thus, as $z\to 0$, $w_h(z)$ is $\mathcal{O}(z^\alpha)$, $\alpha\geq 1$, and similarly, as $z\to 1$, $w_h(z)$ is $\mathcal{O}((1-z)^\beta)$, $\beta\geq 1$. The inner product weight assignment $\omega(z)=(\phi'(z))^{-1/2}=\sqrt{z(1-z)}$ is adequate to nullify the first end-point contribution. In the second end-point term, the chain rule has been used to rewrite the z-derivative of $S_j(z)$ as $\phi'(dS(j,h)\circ\phi(z)/d\phi)$. As z approaches 0 and 1, the first derivative of the sinc function is not defined. However, since $w_h(z)$ is expanded in terms of composite sinc functions with expansion weight $1/\phi'(z)=z(1-z)$, the same choice of inner product weight, $\omega(z)=(\phi'(z))^{-1/2}=\sqrt{z(1-z)}$ leads to the inequalities

$$|S_j(z)\omega'(z)A_v(z)w_h(z)|\leq C_1\sqrt{z(1-z)}$$

and

$$\left|\frac{dS_j}{d\phi}(z)\phi'(z)\omega(z)A_v(z)w_h(z)\right|\leq C_2\sqrt{z(1-z)}$$

Hence we can be assured that both boundary contributions are zero by choosing $\omega(z)=(\phi'(z))^{-1/2}=\sqrt{z(1-z)}$ as the inner product weight function introduced in Step 1.

It should be pointed out that the choice $\omega(z)=(\phi'(z))^{-1}=z(1-z)$ is more general and, in the literature describing sinc function analysis, it is the conventional selection in tutorial problems with mixed boundary conditions. On the other hand, with the assumption of finite reduced velocity shear, the proposed weight not only does the job, it leads to a simpler system to be solved.

Step 3

After carrying out the operations in the integrand (3.9), including evaluations of the derivative combinations of the mapping $\phi(z)=\ln(z/(1-z))$, the integral J can be expressed as

$$J = \int_0^1 \left\{ -\frac{\mathrm{d}^2 S_j(z)}{\mathrm{d}\phi^2} + \frac{1}{4} S_j(z) \right\} A_{\mathrm{v}}(z)(\phi'(z))^{3/2} w_{\mathrm{h}}(z)\, \mathrm{d}z + \int_0^1 \left\{ -\frac{\mathrm{d}S_j(z)}{\mathrm{d}\phi} + \frac{1}{2}(2z-1) S_j(z) \right\} A'_{\mathrm{v}}(z)(\phi'(z))^{1/2} w_{\mathrm{h}}(z)\, \mathrm{d}z \tag{3.10}$$

With J represented by Equation (3.10), after some arrangement of terms, (3.8) can be written in a form convenient for quadrature estimation

$$c_{-N-1} \int_0^1 \{LB_0(z)\} S_j(z)(\phi'(z))^{-1/2}\, \mathrm{d}z + J - \mathrm{i}2\kappa^2 \int_0^1 S_j(z)(\phi'(z))^{1/2} w_{\mathrm{a}}(z)\, \mathrm{d}z + c_{N+1} \int_0^1 \{LB_1(z)\} S_j(z)(\phi'(z))^{-1/2}\, \mathrm{d}z = \int_0^1 F(z) S_j(z)(\phi'(z))^{1/2}\, \mathrm{d}z \tag{3.11}$$

Step 4

The integrals in Equation (3.11) are approximated using the sinc trapezoidal quadrature rule. Specializing Theorem A.3 of Appendix A to the mapping function $\phi(z) = \ln(z/(1-z))$ and adopting 'the layman's choices' for the parameters in the error terms ($\alpha = 1$ and $d = \pi/2$), the sinc quadrature rule is

$$\int_0^1 F(z)\, \mathrm{d}z = h \sum_{k=-N}^{N} \frac{F(z_k)}{\phi'(z_k)} + \mathcal{O}(\mathrm{e}^{-\pi\sqrt{N/2}}) \tag{3.12}$$

where $h = \pi/\sqrt{2N}$ and $z_k = \mathrm{e}^{kh}/(\mathrm{e}^{kh}+1)$ are the nodal points corresponding to a uniform grid of kh operated on by the inverse of the mapping function ϕ. The special case of the rule (A.11) given in Corollary A.1 of Appendix A becomes

$$\int_0^1 G(z) S(j,h) \circ \phi(z)\, \mathrm{d}z = h \frac{G(z_j)}{\phi'(z_j)} + \mathcal{O}(\mathrm{e}^{-\pi\sqrt{N/2}}) \tag{3.13}$$

Consider first the approximation of the integral J and begin by applying (3.12) to the integrals involving the ϕ derivatives of S_j. These are readily evaluated using $\delta_{jk}^{(p)}$, which represents the pth derivative of $S(j,h) \circ \phi(z)$ with respect to ϕ evaluated at z_k. Explicit expressions for these quantities for $p = 0$, 1, and 2 are recorded in (A.5)–(A.7) respectively of Appendix A. Use of these representations leads to the final approximation for J (using the nodal points z_j)

$$J \approx h \sum_{k=-N}^{N} \left\{ -\frac{1}{h^2} \delta_{jk}^{(2)} + \frac{1}{4} \delta_{jk}^{(0)} \right\} A_{\mathrm{v}}(z_k)(\phi'(z_k))^{1/2} w_{\mathrm{h}}(z_k) + h \sum_{k=-N}^{N} \left\{ -\frac{1}{h} \delta_{jk}^{(1)} + \frac{1}{2}(2z_k - 1) \delta_{jk}^{(0)} \right\} A'_{\mathrm{v}}(z_k)(\phi'(z_k))^{-1/2} w_{\mathrm{h}}(z_k) \tag{3.14}$$

for $j = -N-1,\ -N, \ldots,\ N,\ N+1$. From Equation (3.6) and the interpolation property of the sinc basis, one has $w_h(z_k) = c_k/\phi'(z_k)$, which in conjunction with (3.13) provides the approximation of the remaining integrals in (3.11). Using (3.14) in this result, one arrives at the following system of $m = 2N+3$ linear equations whose solution gives the coefficients of the expansion (3.2) for $w_a(z)$. For $j = -N-1,\ -N, \ldots,\ 0, \ldots,\ N,\ N+1$

$$\frac{LB_0(z_j)}{(\phi'(z_j))^{3/2}}\, c_{-N-1} + \sum_{k=-N}^{N} \left\{ -\frac{1}{h^2}\,\delta_{jk}^{(2)} + \frac{1}{4}\,\delta_{jk}^{(0)} \right\} A_v(z_k)(\phi'(z_k))^{-1/2} c_k$$
$$+ \sum_{k=-N}^{N} \left\{ -\frac{1}{h}\,\delta_{jk}^{(1)} + \frac{1}{2}(2z_k - 1)\delta_{jk}^{(0)} \right\} A_v'(z_k)(\phi'(z_k))^{-3/2} c_k + \frac{LB_1(z_j)}{(\phi'(z_j))^{3/2}}\, c_{N+1}$$
$$- \mathrm{i}2\kappa^2(\phi'(z_j))^{-3/2} w_a(z_j) = \frac{F(z_j)}{(\phi'(z_j))^{3/2}} \tag{3.15}$$

The numerators in the boundary terms of (3.15) are

$$LB_0(z) = -\frac{\mathrm{d}}{\mathrm{d}z}\left(A_v(z)\,\frac{\mathrm{d}B_0}{\mathrm{d}z} \right) = 6\,\frac{\mathrm{d}}{\mathrm{d}z}\,(A_v(z)z(1-z)) = 6(A_v(z)(1-2z) + A_v'(z)z(1-z))$$

and

$$LB_1(z) = -\frac{\mathrm{d}}{\mathrm{d}z}\left(A_v(z)\,\frac{\mathrm{d}B_1}{\mathrm{d}z} \right) = -\frac{\mathrm{d}}{\mathrm{d}z}\,(A_v(z)(2-\gamma z)z)$$
$$= -(2A_v(z)(1-\gamma z) + A_v'(z)z(2-\gamma z)z)$$

Step 5

Since (3.15) is a linear system for the expansion coefficients, it is advantageous to rewrite it using matrix notation. Introduce the column vectors

$$\boldsymbol{c} \equiv [c_{-N-1} \quad c_{-N} \quad \cdots \quad c_N \quad c_{N+1}]^T$$

and

$$\boldsymbol{F} \equiv [F(z_{-N-1}) \quad F(z_{-N}) \quad \cdots \quad F(z_N) \quad F(z_{N+1})]^T$$

where $F(z)$ is given in (2.14). Next, for any size define the Toeplitz (constant diagonal) matrices $I^{(p)} \equiv [\delta_{jk}^{(p)}]$, $p = 0, 1, 2$, and the square diagonal matrix $\mathscr{D}(g)$, whose diagonal entries are $g(z_j)$. The elements of the $(2N+3)\times(2N+1)$ matrices $I^{(1)}$ and $I^{(2)}$ are the sinc delta functions $\delta_{jk}^{(1)}$ and $\delta_{jk}^{(2)}$ respectively, and the $(2N+3)\times(2N+1)$ matrix $\mathscr{I}^{(0)}$ is the $(2N+1)\times(2N+1)$ identity matrix with one additional top row and one additional bottom row consisting of zeros. The form of Equation (3.15), for $j = -N-1,\ -N, \ldots,\ N,\ N+1$, suggests the definition of the non-square $(2N+3)\times(2N+1)$ matrix

$$\mathscr{A}_{\mathrm{ns}} \equiv \left\{ -\frac{1}{h^2} I^{(2)} + \frac{1}{4} \mathscr{I}^{(0)} \right\} \mathscr{D}\left(\frac{A_{\mathrm{v}}}{(\phi')^{1/2}} \right) + \left\{ -\frac{1}{h} I^{(1)} + \frac{1}{2} \mathscr{I}^{(0)} \mathscr{D}(2z-1) \right\} \mathscr{D}\left(\frac{A_{\mathrm{v}}}{(\phi')^{3/2}} \right)$$

and the $(2N+3) \times 1$ column vectors $\boldsymbol{a}_{-N-1}$ and $\boldsymbol{a}_{N+1}$ with jth component

$$[\boldsymbol{a}_{-N-1}]_j \equiv \frac{LB_0(z_j)}{(\phi'(z_j))^{3/2}}, \qquad [\boldsymbol{a}_{N+1}]_j \equiv \frac{LB_1(z_j)}{(\phi'(z_j))^{3/2}} \tag{3.16}$$

To build the final system for the unknown coefficients in $\boldsymbol{c}$, we introduce the $m \times m$ $(m = 2N+3)$ bordered matrix

$$\mathscr{B}_{\mathrm{b}} \equiv [\boldsymbol{a}_{-N-1} | \mathscr{A}_{\mathrm{ns}} | \boldsymbol{a}_{N+1}] \tag{3.17}$$

Equation (3.15) can now be expressed compactly as

$$\mathscr{A}_{\mathrm{b}} \boldsymbol{c} \equiv \left(\mathscr{B}_{\mathrm{b}} - \mathrm{i}2\kappa^2 \mathscr{D}\left(\frac{1}{(\phi')^{3/2}} \right) \mathscr{E}_{\mathrm{b}} \right) \boldsymbol{c} = \mathscr{D}\left(\frac{1}{(\phi')^{3/2}} \right) \boldsymbol{F} \tag{3.18}$$

where the $m \times m$ 'evaluator matrix'

$$\mathscr{E}_{\mathrm{b}} \equiv \left[B_0(z_j) \left| \mathscr{I}^{(0)} \mathscr{D}\left(\frac{1}{\phi'} \right) \right| B_1(z_j) \right] \tag{3.19}$$

has been introduced. The complex transformed velocity is recovered from $\boldsymbol{w}_{\mathrm{a}} = \mathscr{E}_{\mathrm{b}} \boldsymbol{c}$, where here $\mathscr{D}(1/\phi')$ is $(2N+1) \times (2N+1)$.

The solution for $w_{\mathrm{a}}(z_j)$ at the nodal point $z_j = \mathrm{e}^{jh}/(1+\mathrm{e}^{jh})$ is constructed as follows. Since $S(k,h) \circ \phi(z_j) = \delta_{jk}^{(0)}$, expansion (3.2), evaluated at the nodal points, is simply

$$w_{\mathrm{a}}(z_j) = c_{-N-1} B_0(z_j) + c_j \frac{1}{\phi'(z_j)} + c_{N+1} B_1(z_j) \tag{3.20}$$

It follows that the solution for $\boldsymbol{w}_{\mathrm{a}}$ at the nodal points are the elements of the column vector

$$\boldsymbol{w}_{\mathrm{a}} = \mathscr{E}_{\mathrm{b}} \boldsymbol{c} = \mathscr{E}_{\mathrm{b}} \mathscr{A}_{\mathrm{b}}^{-1} \mathscr{D}\left(\frac{1}{(\phi')^{3/2}} \right) \boldsymbol{F} \tag{3.21}$$

Thus, Step 5 leads to a solution for the column vectors $\mathrm{Re}(\boldsymbol{w}_{\mathrm{a}})$ and $\mathrm{Im}(\boldsymbol{w}_{\mathrm{a}})$, which are related to the approximate non-dimensional current components evaluated at the nodal points by

$$U_{\mathrm{a}}(z_j) = [\mathrm{Re}(\boldsymbol{w}_{\mathrm{a}})]_j + \kappa(1+\sigma-z_j)\cos(\chi) = u_{\mathrm{a}}(z_j) + \kappa(1+\sigma-z_j)\cos(\chi) \tag{3.22}$$

and

$$V_{\mathrm{a}}(z_j) = [\mathrm{Im}(\boldsymbol{w}_{\mathrm{a}})]_j + \kappa(1+\sigma-z_j)\sin(\chi) = v_{\mathrm{a}}(z_j) + \kappa(1+\sigma-z_j)\sin(\chi) \tag{3.23}$$

Note that, if so desired current components may be computed at evenly spaced grid points using (3.2) with the coefficients obtained from the solution of (3.18).

Recalling the expansion in (3.2), the velocity can also be written as

$$W_a(z) = c_{-N-1}B_0(z) + \sum_{k=-N}^{N} c_k \frac{S(k,h)\circ\phi(z)}{\phi'(z)} + c_{N+1}B_1(z) + \kappa(1+\sigma-z)(\cos(\chi)+\mathrm{i}\ \sin(\chi)) \tag{3.24}$$

where $U_a(z)$ and $V_a(z)$ are the real and imaginary parts of $W_a(z)$ respectively.

4. NUMERICAL TESTING: CONSTANT EDDY VISCOSITY

Determinations of accuracy and computational speed of the Sinc–Galerkin method when applied to the constant eddy viscosity case are described next. These simulations and the illustrative examples that follow later, which are carried out using parameters similar to those that have been used in earlier studies. For purposes of later comparison we will use SI units exclusively.

Since the governing equations and variables in subsequent developments were non-dimensionalized, the only operative constants in (2.13)–(2.16) are κ, σ, and χ. In relating these parameters to the 'constants of nature', we adopt the following nominal values: $|f| = 0.0001$ s^{-1} (appropriate to temperate latitudes), seawater density $\rho = 1.025 \times 10^3$ $\mathrm{kg\,m}^{-3}$, and air density $\rho_{\mathrm{air}} = 1.25$ $\mathrm{kg\,m}^{-3}$. Surface wind stress is assumed to be related to the square of the wind speed W (W in $\mathrm{m\,s}^{-1}$) by

$$\tau_w = C_D \rho_{\mathrm{air}} W^2 \tag{4.1}$$

where the dimensionless parameter $C_D \approx 0.0012$ for $W < 12$ $\mathrm{m\,s}^{-1}$, thereafter increasing linearly to about 0.0025 at gale force winds ($W \approx 30$ $\mathrm{m\,s}^{-1}$) [15]. In keeping with References [3,7], the linear slip bottom stress coefficient k_f is assigned a value of 0.002 $\mathrm{m\,s}^{-1}$ for comparison with other work and to dramatize the change in current speed over the water column. In practice, a value of k_f lower by an order of magnitude may be preferred. Field evidence suggests that the near-surface value of the vertical eddy viscosity is related to the wind speed. In Reference [8], DJT Carter is mentioned as suggesting that, if the wind is not fetch-limited and the sea state is fully developed, then $A_v^*(0)$ in units of $\mathrm{m}^2\,\mathrm{s}^{-1}$ is given by

$$A_v^*(0) \approx 0.304 \times 10^{-4}\, W^3 \tag{4.2}$$

Table I shows values of C_D, the wind stress τ_w ($\mathrm{N\,cm}^{-2}$), the kinematic surface eddy viscosity $A_v^*(0)$ ($\mathrm{m}^2\,\mathrm{s}^{-1}$), the Ekman depth D_E (m), and the seabed depth D_0 (m) (when $\kappa = 10$) corresponding to wind speeds ranging from 10 to 25 $\mathrm{m\,s}^{-1}$.

With the parameters and relationships above, and keeping in mind our desire to compare results with those in Reference [14], we choose our constant eddy viscosity to be

Table I. Parameter values corresponding to a range of wind speeds.

Wind, W (m s^{-1})	10.0	12.0	14.0	16.0	18.0	20.0	25.0
C_D	0.0012	0.0012	0.00134	0.00149	0.00163	0.00178	0.00214
τ_w (N m^{-2})	0.15	0.22	0.33	0.48	0.66	0.89	1.67
$A_v^*(0)$ (m^2 s^{-1})	0.0304	0.0526	0.0835	0.1246	0.1775	0.2434	0.4755
D_E (m)	24.7	32.4	40.9	49.9	59.6	69.8	97.5
D_0 (m) ($\kappa = 10$)	247.0	324.0	409.0	499.0	596.0	698.0	975.0

$$A_v^*(z^*) \equiv 0.02 \text{ m}^2 \text{ s}^{-1} \tag{4.3}$$

with $\tau_w = \sqrt{2}/10 = 0.1414$ N m^{-2}. From Table I, the wind speed W may be inferred to be about 9 m s^{-1}. Since $D_E = \sqrt{2A_v^*(0)/|f|} = 20$ m, we then have $\kappa = D_0/D_E = D_0/20$. In keeping with Reference [14], we will use $D_0 = 100$ m and hence $\kappa = 5$, which it will be throughout.

The numerical results will be compared with the exact solution $W(z) = U_0[U(z) + iV(z)]$, where $U(z)$ is given by

$$U(z) = \text{Re}(W_c(z))\cos(\chi) - \text{Im}(W_c(z))\sin(\chi)$$

and $V(z)$ is given by

$$V(z) = \text{Re}(W_c(z))\sin(\chi) + \text{Im}(W_c(z))\cos(\chi)$$

Here $\text{Re}(W_c(z))$ and $\text{Im}(W_c(z))$ denote the real and imaginary parts of $W_c(z)$ respectively, and

$$W_c(z) = \frac{\kappa(1-i)\sigma\cosh(\kappa(1-i)(1-z)) + \sinh(\kappa(1-i)(1-z))}{(1-i)[\cosh(\kappa(1-i)) + \kappa(1-i)\sigma\sinh(\kappa(1-i))]}$$

The results of the Sinc–Galerkin approximations $U_a(z_j)$ and $V_a(z_j)$ were compared with the exact solutions for $U(z_j)$ and $V(z_j)$ at the sinc grid points

$$\mathscr{S} = \{z_j = \phi^{-1}(jh) = e^{jh}/(e^{jh} + 1):\ j = -N-1, \ldots, N+1\} \tag{4.4}$$

These results were then multiplied by the natural velocity scale U_0 to give a dimensional representation of the velocities.

All numerical simulations were run on a SUN Ultra 5 workstation with MATLAB Version 5.2. To illustrate the performance of the method, the maximum absolute errors are reported as

$$\|U_{\mathscr{S}}\| = \max_{-N-1 \le j \le N+1}\{U_0|U_a(z_j) - U(z_j)|\} \tag{4.5}$$

$$\|V_{\mathscr{S}}\| = \max_{-N-1 \le j \le N+1}\{U_0|V_a(z_j) - V(z_j)|\} \tag{4.6}$$

and

$$\|E_{\mathscr{S}}\| = \max\{\|U_{\mathscr{S}}\|,\ \|V_{\mathscr{S}}\|\} \tag{4.7}$$

where the units are m s^{-1}. Computation times are reported as CPU (in s) and were calculated using the MATLAB command CPUTIME.

Throughout, comparable graphs (of eddy viscosity functions and velocity components) are shown on the same scale. This way visual comparisons of these various quantities are readily made.

Example 4.1

For this example (constant eddy viscosity) we choose $\chi = 45°$ and for the linear stress condition at the seabed we have $\sigma = A_v^*(D_0)/(k_f D_0) = 0.1$. The value of N then corresponds to a discrete system of size $m \times m$ ($m = 2N + 3$), given in (3.18). The errors and CPU times are given in Table II and show a high degree of accuracy with minimal computational cost.

Figure 1 graphically depicts the numerical convergence of the Sinc–Galerkin method to the exact solution with the linear stress bottom boundary condition, as N is repeatedly doubled in size. The horizontal projection of the Ekman spiral for $N = 64$ is indistinguishable from the true solution shown as the solid line.

Example 4.2

In this example we replace the linear stress bottom boundary condition with a no-slip condition at the seabed to test the dependence of this scheme on the parameter σ. This is accomplished by setting $\sigma = 0$ in the original formulation. All other parameters remain the same. The same discrete system given in (3.18) is used and again the value of N corresponds to a discrete system of size $m \times m$ ($m = 2N + 3$). The errors and CPU times are given in Table III for the same oceanographic conditions and show similar, remarkably accurate results. For a depth of 100 m, the surface projections of the Ekman spirals are very nearly the same, and for $N = 64$ are indistinguishable from the true solution.

Table II. Errors for Example 4.1 (constant eddy viscosity) on the sinc grid $\mathscr{S}$ with the linear stress bottom condition for $\sigma = 0.1$, $\chi = 45°$, $\kappa = 5$ ($D_0 = 100$ m, $D_E = 20$ m).

N	m	CPU (s)	$\|U_{\mathscr{S}}\|$ (m s^{-1})	$\|V_{\mathscr{S}}\|$ (m s^{-1})	$\|E_{\mathscr{S}}\|$ (m s^{-1})
4	11	0.01	1.10×10^{-3}	7.48×10^{-4}	1.10×10^{-3}
8	19	0.01	2.50×10^{-4}	1.29×10^{-4}	2.50×10^{-4}
16	35	0.03	2.76×10^{-5}	1.30×10^{-5}	2.76×10^{-5}
32	67	0.15	8.99×10^{-7}	4.24×10^{-7}	8.99×10^{-7}
64	131	1.01	5.78×10^{-9}	2.78×10^{-9}	5.78×10^{-9}
128	259	10.19	4.08×10^{-12}	1.97×10^{-12}	4.08×10^{-12}

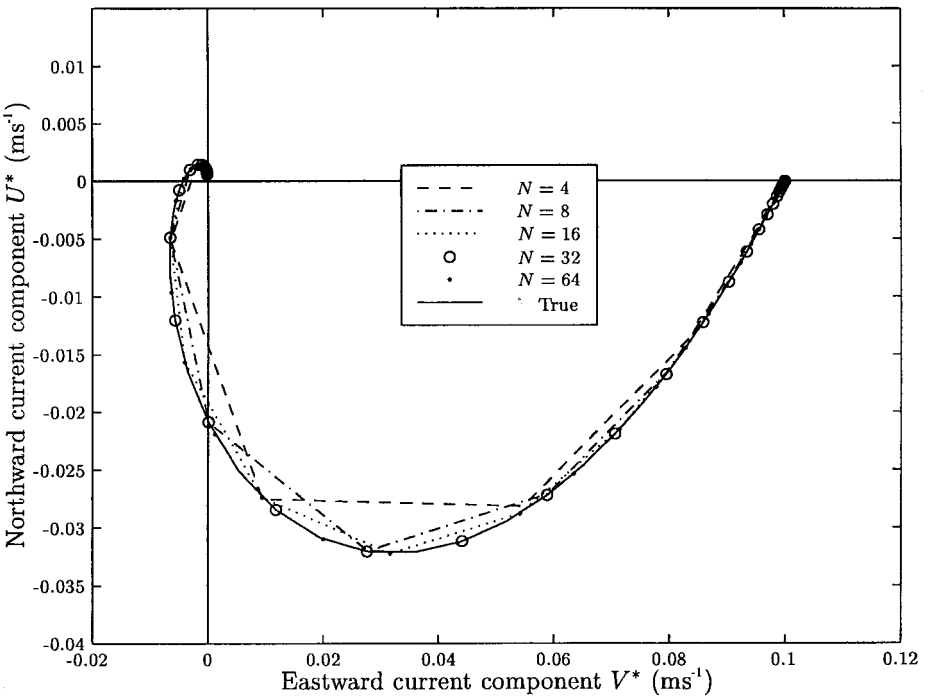

Figure 1. Sinc–Galerkin Ekman spiral projections for Example 4.1 with increasing N for the case of constant eddy viscosity with linear stress bottom boundary ($\sigma = 0.1$, $\chi = 45°$, $\kappa = 5$, $D_0 = 100$ m, $D_E = 20$ m).

Table III. Errors for Example 4.2 on the sinc grid $\mathscr{S}$ with the zero-velocity bottom condition (no-slip) for $\sigma = 0$, $\chi = 45°$, $\kappa = 5$ ($D_0 = 100$ m, $D_E = 20$ m).

N	m	CPU (s)	$\|U_{\mathscr{S}}\|$ (m s^{-1})	$\|V_{\mathscr{S}}\|$ (m s^{-1})	$\|E_{\mathscr{S}}\|$ (m s^{-1})
4	11	0.01	1.10×10^{-3}	7.50×10^{-4}	1.10×10^{-3}
8	19	0.01	2.48×10^{-4}	1.30×10^{-4}	2.48×10^{-4}
16	35	0.03	2.75×10^{-5}	1.31×10^{-5}	2.75×10^{-5}
32	67	0.16	8.96×10^{-7}	4.26×10^{-7}	8.96×10^{-7}
64	131	1.07	5.76×10^{-9}	2.78×10^{-9}	5.76×10^{-9}
128	259	10.13	4.07×10^{-12}	1.98×10^{-12}	4.07×10^{-12}

5. NUMERICAL TESTING: DEPTH-DEPENDENT EDDY VISCOSITY

In seas of shallow-to-intermediate depth, at low wind speeds, various factors, such as vigorous tidal mixing, are expected to lead to maximum values of $A_v^*(z^*)$ at intermediate depths and minimal values near the surface and seabed. On the other hand, over deeper water, turbulence generated by high winds produces relatively large values of $A_v^*(z^*)$ near the surface. In either

case, the Sinc–Galerkin method provides a convenient and efficient means for surveying depth-dependent functions $A_v^*(z^*)$ and for determining the associated sub-surface current distributions. In this section we provide one further numerical test of the accuracy and efficiency of the Sinc–Galerkin method for a decreasing depth-dependent viscosity function. In Section 6 we choose a depth-dependent eddy viscosity function that has maximum values at intermediate depths and minimal values near the surface and seabed. In a sea of depth $D_0 = 100$ m, we choose an eddy viscosity function that decreases quadratically from the values of $A_v^*(0) = 0.02\ \mathrm{m^2\,s^{-1}}$ to the minimum value of $A_v^*(D_0) = 0.00125\ \mathrm{m^2\,s^{-1}}$. This decreasing eddy viscosity function is given by

$$A_v^*(z^*) = 0.02[1 - (0.0075)z^*]^2, \quad 0 < z^* < D_0 = 100\ \mathrm{m} \tag{5.1}$$

A graph of the $A_v^*(z^*)$ in (5.1) is shown in Figure 2, where it is contrasted with a constant eddy viscosity of $A_v^*(z^*) \equiv 0.02\ \mathrm{m^2\,s^{-1}}$.

Again for the purpose of illustrating applications of the Sinc–Galerkin technique, we use parameters from Reference [14], which include a sea of $D_0 = 100$ m depth, a steady breeze of wind stress $\tau_w = 0.14140\ \mathrm{N\,m^{-2}}$, and a surface value of the eddy viscosity of $A_v^*(0) = 0.02\ \mathrm{m^2\,s^{-1}}$. Then from Table I, the wind speed W is the inferred to be about $9\ \mathrm{m\,s^{-1}}$. Since $D_E = \sqrt{2A_v^*(0)/|f|} = 20$ m, we then have $\kappa = D_0/D_E = 5$. The system solved is of size $m \times m$ ($m = 2N + 3$) and is given in (3.18).

The numerical results will be compared with a finite difference solution and with the exact solution $W(z) = U_0[U(z) + iV(z)]$, where $U(z)$ is given by

$$U(z) = \mathrm{Re}(W_d(z))\cos(\chi) - \mathrm{Im}(W_d(z))\sin(\chi)$$

and $V(z)$ is given by

$$V(z) = \mathrm{Re}(W_d(z))\sin(\chi) + \mathrm{Im}(W_d(z))\cos(\chi)$$

Here $\mathrm{Re}(W_d(z))$ and $\mathrm{Im}(W_d(z))$ denote the real and imaginary parts of $W_d(z)$ respectively, and

$$\begin{aligned} W_d(z) = {} & c_1(1+\gamma z)^{\nu-1/2}[\cos(\mu\ln(1+\gamma z)) - i\sin(\mu\ln(1+\gamma z))]\,e^{i\chi} \\ & + c_2(1+\gamma z)^{-\nu-1/2}[\cos(\mu\ln(1+\gamma z)) + i\sin(\mu\ln(1+\gamma z))]\,e^{i\chi} \end{aligned}$$

where

$$c_1 = -A\left(B + \left(\frac{[1-(1/2-\nu)\sigma_1] - i\sigma_1\mu}{[1-(1/2+\nu)\sigma_1] + i\sigma_1\mu}\right)\exp[2(\nu - i\mu)\ln(1+\gamma)]\right)^{-1}$$

and

$$c_2 = A + c_1 B$$

with

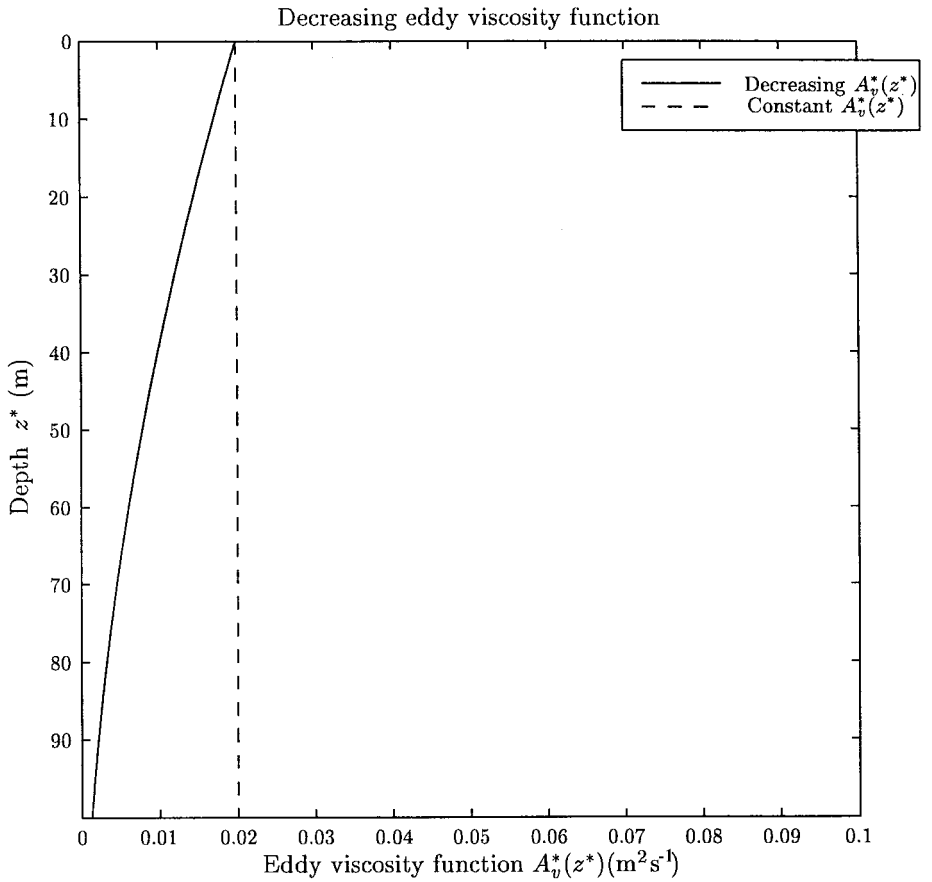

Figure 2. Eddy viscosity functions $A_v^*(z^*) = 0.02[1 - (0.0075)z^*]^2$ and $A_v^*(z^*) \equiv 0.02$.

$$A = \frac{\kappa}{\gamma}\left[\frac{(v+1/2)+\mathrm{i}\mu}{(v+1/2)^2+\mu^2}\right], \qquad B = \frac{(v^2+\mu^2-1/4)-\mathrm{i}\mu}{(v+1/2)^2+\mu^2}, \qquad \sigma_1 = \frac{\sigma\gamma}{1+\gamma}$$

and

$$v - \mathrm{i}\mu = \frac{1}{2}\sqrt{1 - \mathrm{i}8\kappa^2/\gamma^2}$$

The results of the Sinc–Galerkin approximations, $U_a(x_k)$ and $V_a(x_k)$, and the finite difference approximations, $\hat{U}_a(x_k)$ and $\hat{V}_a(x_k)$, were compared with the exact solutions, $U(x_k)$ and $V(x_k)$, on a uniform grid

$$\mathscr{U} = \{x_k = kh_{\mathrm{fd}}:\ k = 0, \ldots, N_{\mathrm{fd}} - 1\} \tag{5.2}$$

where $h_{\mathrm{fd}} = 1/(N_{\mathrm{fd}} - 1)$, N_{fd} being the number of grid points for the finite difference method. This uniform grid is the natural grid for the finite difference method and the Sinc–Galerkin results were determined at these grid points using (3.2) and the coefficients $\{c_j\}$ of the vector $\boldsymbol{c}$. These results were again multiplied by the natural velocity scale U_0 to give a dimensional representation of the velocities. To illustrate the performance of the method, the maximum absolute errors for the Sinc–Galerkin method are reported as

$$\|U_{\mathscr{U}}\| = \max_{0 \le k \le N_{\mathrm{fd}} - 1} \{U_0 |U_{\mathrm{a}}(x_k) - U(x_k)|\}, \qquad \|V_{\mathscr{U}}\| = \max_{0 \le k \le N_{\mathrm{fd}} - 1} \{U_0 |V_{\mathrm{a}}(x_k) - V(x_k)|\}$$

and

$$\|E_{\mathscr{U}}\| = \max\{\|U_{\mathscr{U}}\|,\ \|V_{\mathscr{U}}\|\}$$

where the units are m s^{-1}. The maximum absolute errors for the finite difference method are reported as

$$\|\hat{U}_{\mathscr{U}}\| = \max_{0 \le k \le N_{\mathrm{fd}} - 1} \{U_0 |\hat{U}_{\mathrm{a}}(x_k) - U(x_k)|\}, \qquad \|\hat{V}_{\mathscr{U}}\| = \max_{0 \le k \le N_{\mathrm{fd}} - 1} \{U_0 |\hat{V}_{\mathrm{a}}(x_k) - V(x_k)|\}$$

and

$$\|\hat{E}_{\mathscr{U}}\| = \max\{\|\hat{U}_{\mathscr{U}}\|,\ \|\hat{V}_{\mathscr{U}}\|\}$$

where the units are also m s^{-1}.

Example 5.1

For the example in a sea of depth $D_0 = 100$ m, the parameters are chosen to be $\sigma = 0.1$, $\chi = 45°$, and (since $D_{\mathrm{E}} = 20$ m) $\kappa = 5$. In the tables that are provided we have tried to convey both the exponential convergence of the Sinc–Galerkin method and a brief comparison with a standard finite difference method. No claims of programming efficiency can be made for either code, the comparisons only give a flavor for the relative merits of each method. We first compare with Examples 4.1 and 4.2 using the same sinc grids S given in (4.4). Table IV shows

Table IV. Errors for Example 5.1 on the sinc grid $\mathscr{S}$ with the linear stress bottom condition for $\sigma = 0.1$, $\chi = 45°$, $\kappa = 5$ ($D_0 = 100$ m, $D_{\mathrm{E}} = 20$m).

N	m	CPU (s)	$\|U_{\mathscr{S}}\|$ (m s^{-1})	$\|V_{\mathscr{S}}\|$ (m s^{-1})	$\|E_{\mathscr{S}}\|$ (m s^{-1})
4	11	0.01	1.30×10^{-3}	1.60×10^{-3}	1.60×10^{-3}
8	19	0.02	1.19×10^{-4}	2.35×10^{-4}	2.35×10^{-4}
16	35	0.03	1.56×10^{-5}	2.06×10^{-5}	2.06×10^{-5}
32	67	0.16	7.55×10^{-7}	8.22×10^{-7}	8.22×10^{-7}
64	131	1.14	3.23×10^{-9}	4.96×10^{-9}	4.96×10^{-9}
128	259	10.26	2.08×10^{-12}	2.43×10^{-12}	2.43×10^{-12}

accuracy very similar to that seen when solving the constant viscosity cases of Example 4.1 and 4.2 (compare Table IV with Tables II and III).

Figure 3 shows the Ekman spiral projection for the decreasing eddy viscosity calculated with $N = 128$ in comparison with the same quantity for the constant eddy viscosity. Figure 4 shows the associated depth variations of the components calculated with $N = 128$; the same quantities for the constant eddy viscosity are given for comparison. Ekman spiral projections for increasing N are superimposed in Figure 5, which again conveys the rapid convergence of the sinc method.

A finite difference code using standard second-order differences was implemented. The resulting bi-tridiagonal system is solved with Gauss elimination and back substitution. As a first comparison, Table V shows the numerical results (errors calculated on the uniform grid $\mathscr{U}$ of (5.2)) that can be achieved using the finite difference code and the same discrete system size as the Sinc–Galerkin method (denoted by $m = 2N + 3$). Not surprisingly, the finite difference code runs far faster and is far less accurate. This is an obvious result of the exponential convergence rate of the Sinc–Galerkin method and the resulting discrete system that is full, not sparse.

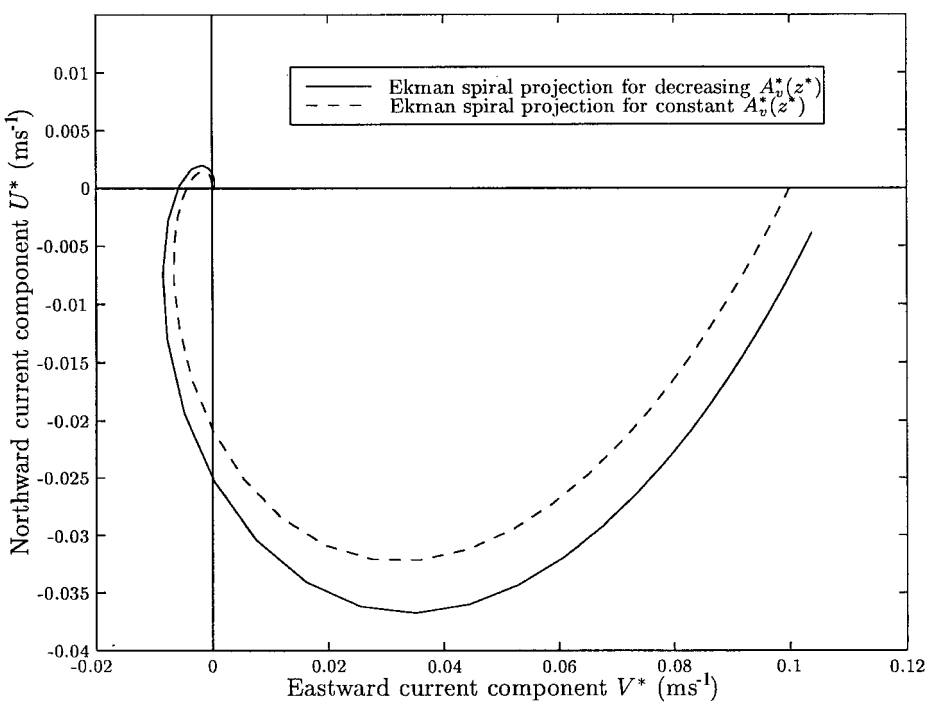

Figure 3. Sinc–Galerkin Ekman spiral projections calculated for constant and decreasing eddy viscosity functions with linear stress bottom boundary.

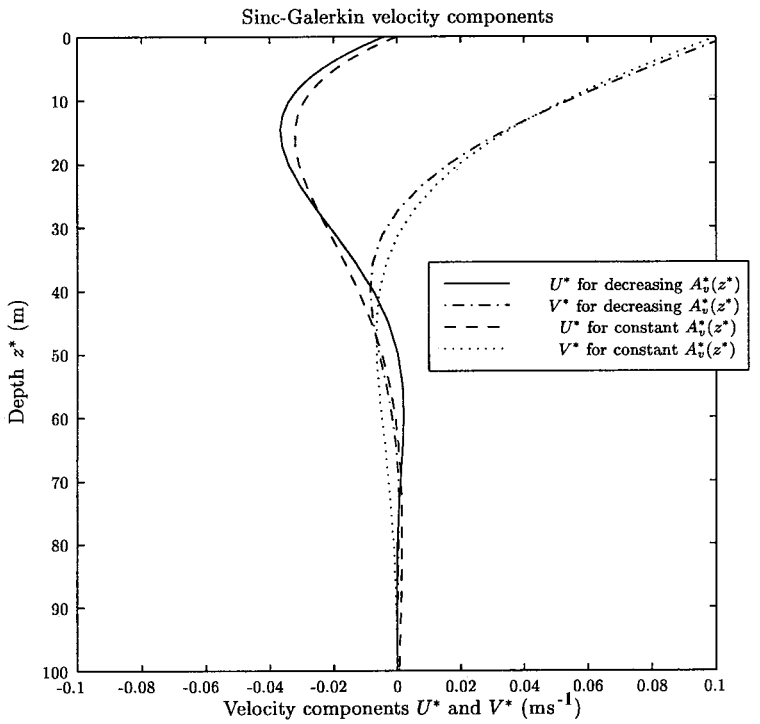

Figure 4. Sinc–Galerkin northward and eastward calculated velocity profiles for constant and decreasing eddy viscosity functions with linear stress bottom boundary.

For another comparison, Table VI shows the numerical results (errors again calculated on the uniform grid $\mathscr{U}$ of (5.2)) that can be obtained using the finite difference code to achieve the same accuracy as the Sinc–Galerkin method. Not surprisingly, the finite difference code requires a far larger discrete system and much more CPU time to achieve the same accuracy.

6. SUB-SURFACE CURRENTS AND DEPTH-DEPENDENT EDDY VISCOSITY

In this section we examine a quadratic viscosity function that is very similar to that derived in the NUBBLE User's Manual [14] via an advanced turbulence closure method. In a sea of depth $D_0 = 100$ m, our eddy viscosity function increases quadratically from the value of $A_v^*(0) = 0.02$ m^2 s^{-1} to the maximum value of $A_v^*(D_0/2) = 0.08$ m^2 s^{-1} and then decreases quadratically again to $A_v^*(D_0) = 0.02$ m^2 s^{-1}. This quadratic eddy viscosity function is given by

$$A_v^*(z^*) = 0.02[1 + (0.12)z^*(1 - (0.01)z^*)], \quad 0 < z^* < D_0 = 100 \text{ m} \tag{6.1}$$

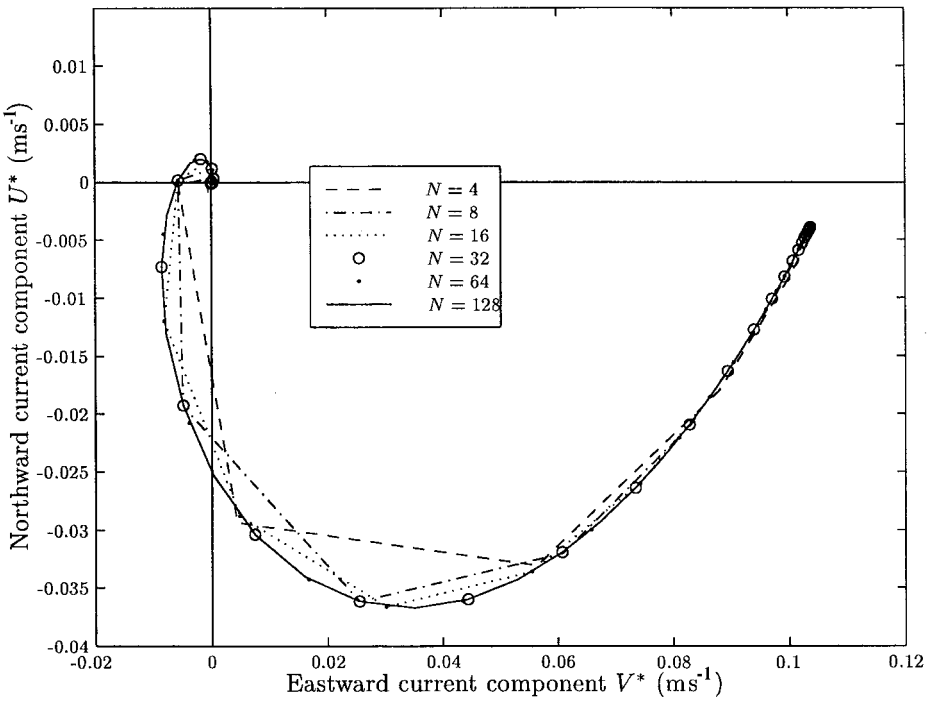

Figure 5. Sinc–Galerkin Ekman spiral projections calculated for increasing N for the case of the decreasing eddy viscosity function with linear stress bottom boundary.

Table V. Comparison of the Sinc–Galerkin method and the finite difference method using the same discrete system size ($m = N_{\mathrm{fd}}$) for Example 5.1[a].

$m = N_{\mathrm{fd}}$	$\|\hat{E}_{\mathscr{U}}\|$ (m s^{-1})	CPU (s)	CPU (s)	$\|E_{\mathscr{U}}\|$ (m s^{-1})
11	6.30×10^{-3}	0.02	0.01	1.60×10^{-3}
19	1.90×10^{-3}	0.04	0.02	2.35×10^{-4}
35	5.41×10^{-4}	0.06	0.03	2.06×10^{-5}
67	1.44×10^{-4}	0.13	0.16	8.22×10^{-7}
131	3.70×10^{-5}	0.25	1.14	4.96×10^{-9}
259	9.40×10^{-6}	0.52	10.26	2.43×10^{-12}

[a] Results are reported on the uniform grid $\mathscr{U}$ with the linear stress bottom condition for $\sigma = 0.1$, $\chi = 45°$, $\kappa = 5$ ($D_0 = 100$ m, $D_{\mathrm{E}} = 20$ m).

Table VI. Comparison of the Sinc–Galerkin method and the finite difference method using the same accuracy achieved for Example 5.1[a].

$\|\hat{E}_{\mathscr{U}}\|$ (m s^{-1})	CPU (s)	N_{fd}	m	CPU (s)	$\|E_{\mathscr{U}}\|$ (m s^{-1})
1.60×10^{-3}	0.04	21	11	0.01	1.60×10^{-3}
2.41×10^{-4}	0.10	52	19	0.02	2.35×10^{-4}
2.07×10^{-5}	0.34	175	35	0.03	2.06×10^{-5}
8.23×10^{-7}	2.07	873	67	0.16	8.22×10^{-7}
4.99×10^{-9}	147.44	11200	131	1.14	4.96×10^{-9}

[a] Results are reported on the uniform grid $\mathscr{U}$ with the linear stress bottom condition for $\sigma = 0.1$, $\chi = 45°$, $\kappa = 5$ ($D_0 = 100$ m, $D_{\mathrm{E}} = 20$ m).

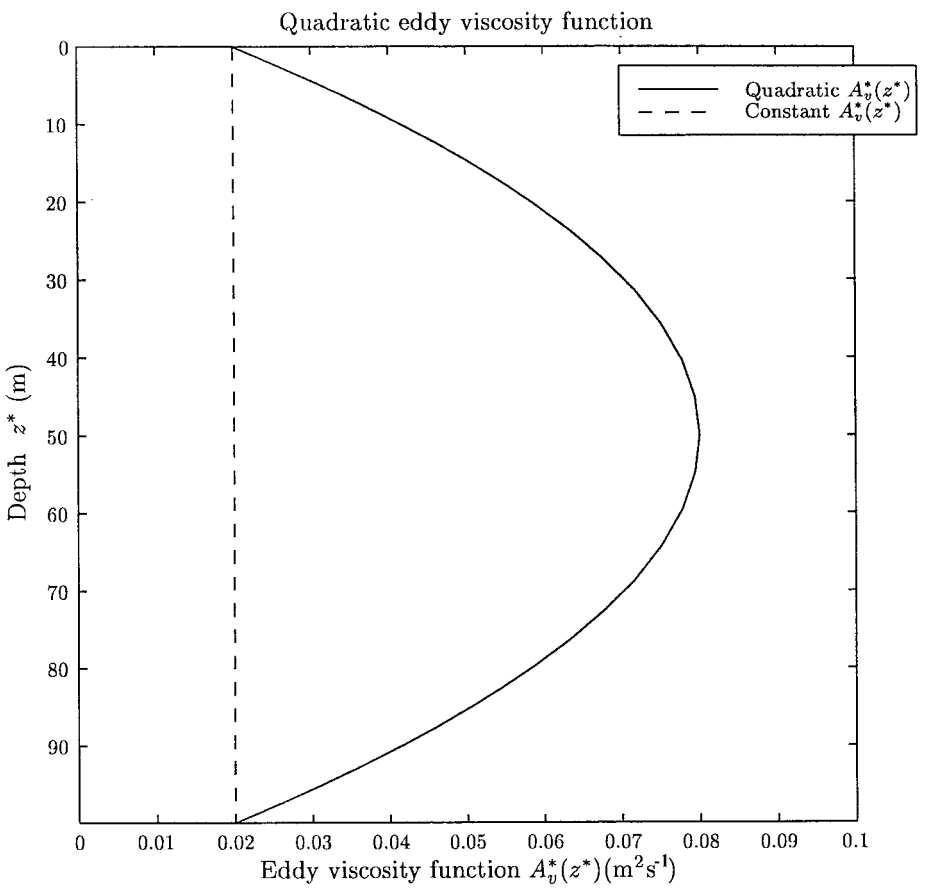

Figure 6. Eddy viscosity functions $A_{\mathrm{v}}^*(z^*) = 0.02[1 + (0.12)z^*(1 - (0.01)z^*)]$ and $A_{\mathrm{v}}^*(z^*) \equiv 0.02$.

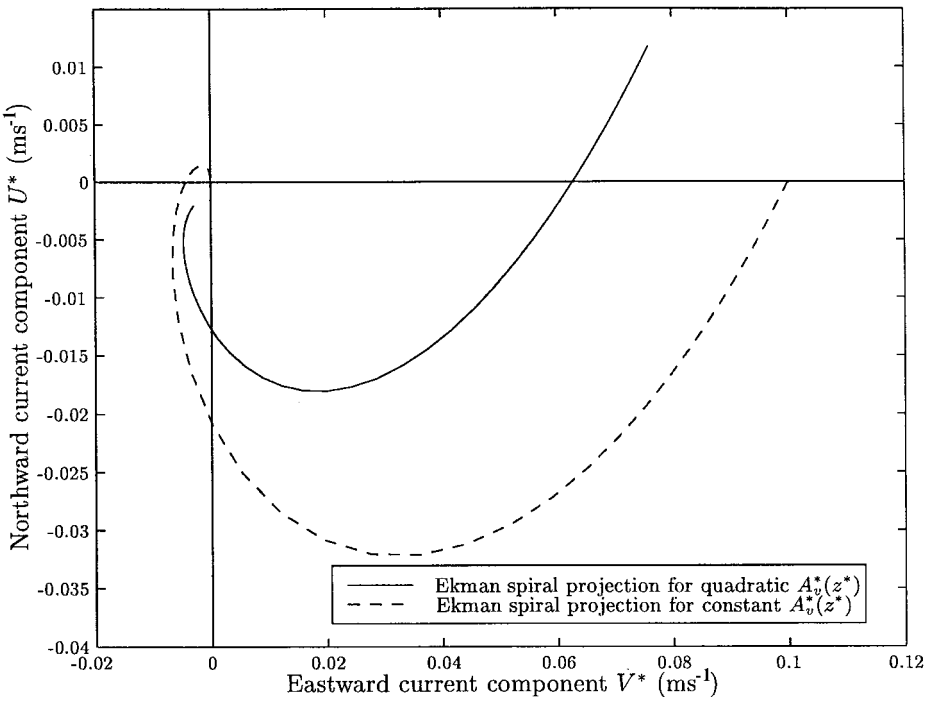

Figure 7. Sinc–Galerkin Ekman spiral projections calculated for constant and quadratic eddy viscosity functions with linear stress bottom boundary.

A graph of the $A_v^*(z^*)$ in (6.1) is shown in Figure 6, where it is contrasted with a constant eddy viscosity of $A_v^*(z^*) \equiv 0.02\ \mathrm{m^2\,s^{-1}}$.

As we have throughout, we use a sea of $D_0 = 100$ m depth, a steady breeze of wind stress $\tau_w = 0.14140\ \mathrm{N\,m^{-2}}$, and a surface value of the eddy viscosity of $A_v^*(0) = 0.02\ \mathrm{m^2\,s^{-1}}$, which allows us to infer from Table I a wind speed W of about 9 m s^{-1}. Again $D_E = \sqrt{2A_v^*(0)/|f|} =$ 20 m and thus $\kappa = D_0/D_E = 5$. The system solved is of size $m \times m$ ($m = 2N + 3$) and is given in (3.18).

Example 6.1

The parameters are again chosen to be $\sigma = 0.1$, $\chi = 45°$, and (since $D_E = 20$ m) $\kappa = 5$. Figure 7 shows the Ekman spiral projections for the quadratic eddy viscosity calculated with $N = 128$ in comparison with the same quantities for the constant eddy viscosity. Figure 8 shows the associated depth variations of the velocity components calculated with $N = 128$; the same quantities for the constant eddy viscosity are given for comparison. Ekman spiral projections for increasing N are superimposed in Figure 9, which again conveys the rapid convergence of the sinc method. A comparison of these results with those in Figure 3.1 of Reference [14] shows remarkably good agreement despite our depth-symmetric approximation of $A_v^*(z^*)$ and use of a linear slip condition.

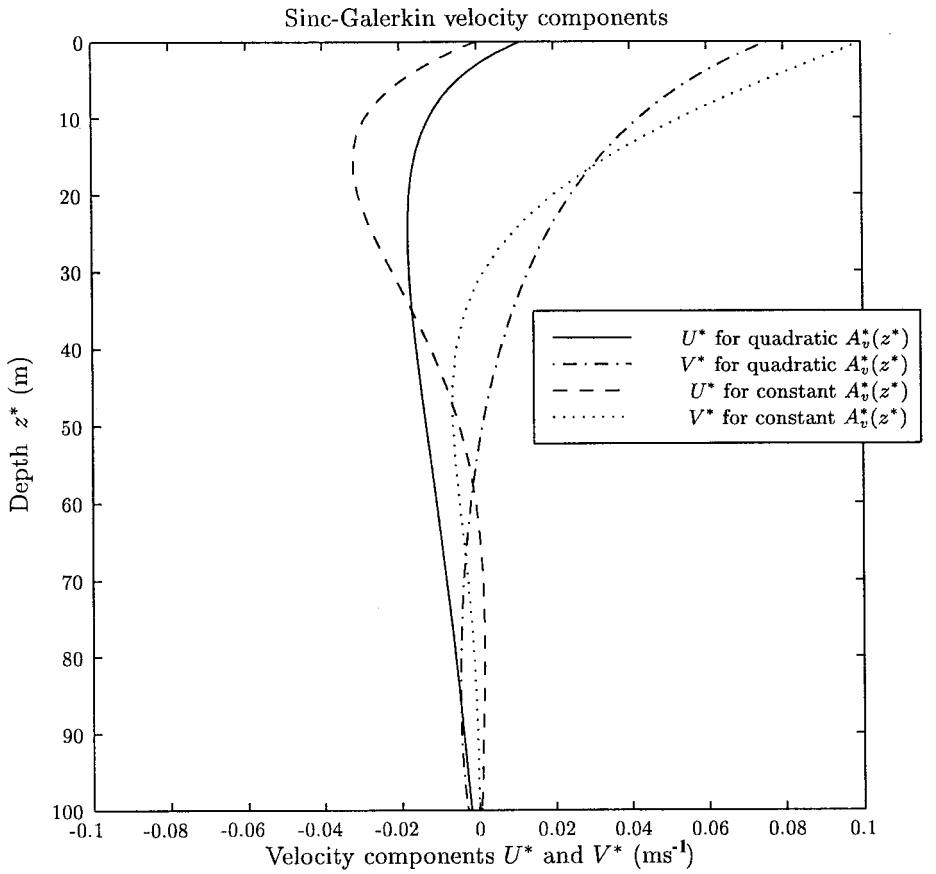

Figure 8. Sinc–Galerkin northward and eastward calculated velocity profiles for constant and quadratic eddy viscosity functions with linear stress bottom boundary.

7. CONCLUSIONS

The Sinc–Galerkin technique is potentially a useful variant of spectral methods in oceanographic problems with boundary layers. It is particularly well suited for such problems inasmuch as the sinc grid points naturally provide the greatest resolution in boundary layer regions. The method also is computationally efficient and accurate, since the properties of sinc functions provide exponentially convergent estimations of the integrals that arise in applications of the Galerkin technique.

Application of the Sinc–Galerkin method to the Ekman wind-driven current problem suggests that sub-surface current distributions are much more profoundly influenced by an increase in vertical eddy viscosity coefficient with depth than by a decrease of $A_v^*(z^*)$ relative

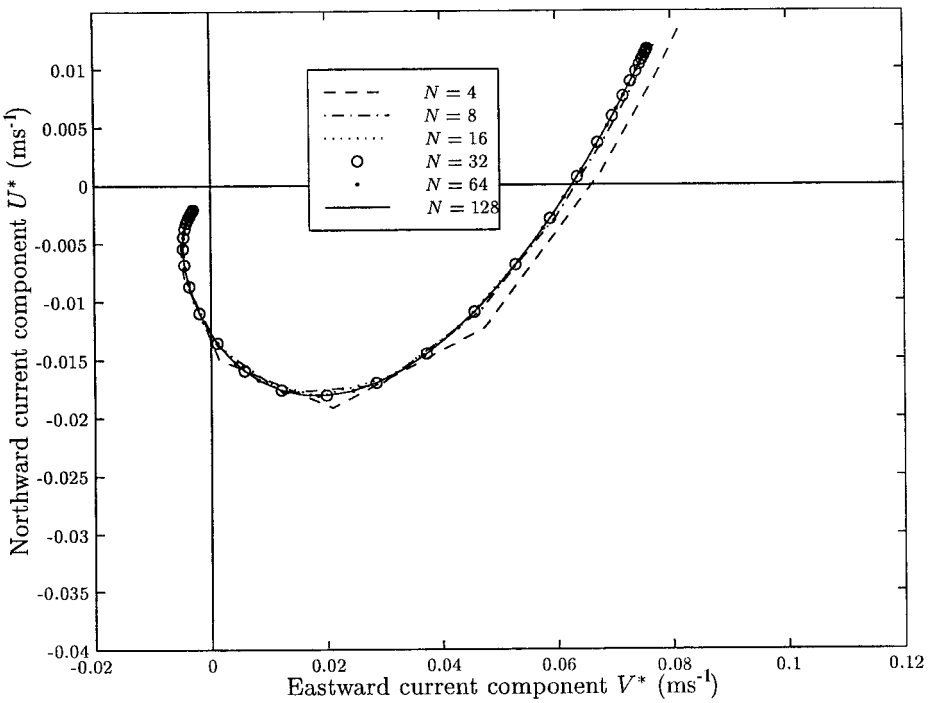

Figure 9. Sinc–Galerkin Ekman spiral projections calculated for increasing N for the case of the quadratic eddy viscosity function with linear stress bottom boundary.

to a constant $A_v^*(z^*)$. This difference seems sufficiently pronounced that the inverse problem, e.g. field measurements of current and pressure to infer the depth dependence of the vertical eddy viscosity coefficient when $A_v^*(z^*)$ decreases with depth from its surface value, is unlikely to yield results that are quantitatively significant.

Additional advantages of expansions with appropriate composite sinc functions may emerge when applied to problems with coastal boundaries and, in particular, to spin-up problems, where the Sinc–Galerkin technique provides an attractive alternative to time marching methods.

ACKNOWLEDGMENTS

This paper was supported in part by Research Corporation Science Award # CC4385 and a summer research grant from the University of Redlands.

APPENDIX A. SINC FUNCTION FUNDAMENTALS

A through review of sinc function properties and the general Sinc–Galerkin method can be found in References [10–12]; this appendix contains an overview of those properties which are employed when developing techniques for the solution of differential equations.

A.1. The sinc function

The sinc function is defined on the whole real line, $-\infty < t < \infty$, by

$$\operatorname{sinc}(t) \equiv \begin{cases} \dfrac{\sin(\pi t)}{\pi t}, & t \neq 0 \\ 1, & t = 0 \end{cases} \tag{A.1}$$

For $h > 0$, translated sinc functions with evenly spaced nodes are given by

$$S(k, h)(t) \equiv \operatorname{sinc}\left(\frac{t - kh}{h}\right), \quad k = 0, \pm 1, \pm 2, \ldots \tag{A.2}$$

If a function $f(t)$ is defined on the real axis, then for $h > 0$, the series

$$C(f, h)(t) = \sum_{k=-\infty}^{\infty} f(kh) \operatorname{sinc}\left(\frac{t - kh}{h}\right)$$

is called the Whittaker cardinal expansion of f whenever this series converges. The properties of Whittaker cardinal expansions have been studied and are thoroughly surveyed in Lund and Bowers [10]. These properties are derived in the infinite strip $\mathscr{D}_S$ of the complex w-plane, where for $d > 0$

$$\mathscr{D}_S = \left\{ w = t + \mathrm{i}s\colon\ |s| < d \leq \frac{\pi}{2} \right\} \tag{A.3}$$

Approximations can be constructed for infinite, semi-infinite, and finite intervals. To construct approximations on the interval (0, 1), which is used in this paper, the eye-shaped domain in the z-plane

$$\mathscr{D}_E = \left\{ z = x + \mathrm{i}y\colon\ \left|\arg\left(\frac{z}{1 - z}\right)\right| < d \leq \frac{\pi}{2} \right\}$$

is mapped conformally onto the infinite strip $\mathscr{D}_S$ via

$$w = \phi(z) = \ln\left(\frac{z}{1 - z}\right)$$

(see Figure A1) and this is a suitable domain for the Sinc–Galerkin method. The basis functions on (0, 1) are taken to be the composite translated functions

$$S(k, h) \circ \phi(z) \equiv \operatorname{sinc}\left(\frac{\phi(z) - kh}{h}\right)$$

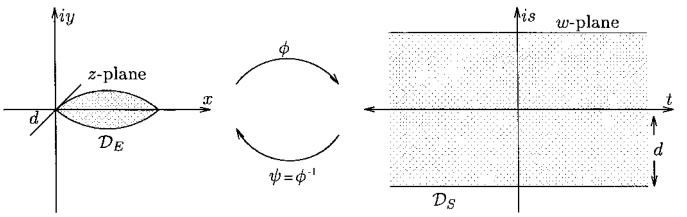

Figure A1. Relationship between the domains $\mathscr{D}_{\mathrm{E}}$ and $\mathscr{D}_{\mathrm{S}}$.

Comparison of this form with (A.2) shows that t has simply been replaced by $\phi(z)$.

The inverse map of $w=\phi(z)$ is $\phi^{-1}(w)=\psi(w)=\mathrm{e}^{w}/(1+\mathrm{e}^{w})$. Thus, we may define the inverse images of the real line and of the evenly spaced nodes $\{kh\}_{k=-\infty}^{\infty}$ as

$$\Gamma=\{\psi(t)\in\mathscr{D}_{\mathrm{E}}:\ -\infty<t<\infty\}$$

and

$$z_k=\psi(kh)=\frac{\mathrm{e}^{kh}}{1+\mathrm{e}^{kh}},\quad k=0,\ \pm 1,\ \pm 2,\ldots \tag{A.4}$$

respectively. For $h^{*}=\pi/8$, three adjacent members of this basis $S(k,h)\circ\phi(z)$, $k=-1,0,1$, are graphed for the values $x=\mathrm{Re}(z)$, $0<x<1$, and are shown in Figure A2.

The Sinc–Galerkin method requires derivatives of composite sinc functions evaluated at the nodes. The conventional notation for the pth derivative of $S(j,h)\circ\phi(z)$ with respect to ϕ evaluated at the nodal point z_k is

$$\frac{1}{h^{p}}\,\delta_{jk}^{(p)}\equiv\frac{\mathrm{d}^{p}}{\mathrm{d}\phi^{p}}\left[S(j,h)\circ\phi(z)\right]\Big|_{z=z_k}$$

The expressions required for the present discussion are

$$\delta_{jk}^{(0)}\equiv\left[S(j,h)\circ\phi(z)\right]\big|_{z=z_k}=\begin{cases}1, & k=j\\ 0, & k\neq j\end{cases} \tag{A.5}$$

$$\delta_{jk}^{(1)}\equiv h\,\frac{\mathrm{d}}{\mathrm{d}\phi}\left[S(j,h)\circ\phi(z)\right]\Big|_{z=z_k}=\begin{cases}0, & k=j\\ \dfrac{(-1)^{k-j}}{k-j}, & k\neq j\end{cases} \tag{A.6}$$

and

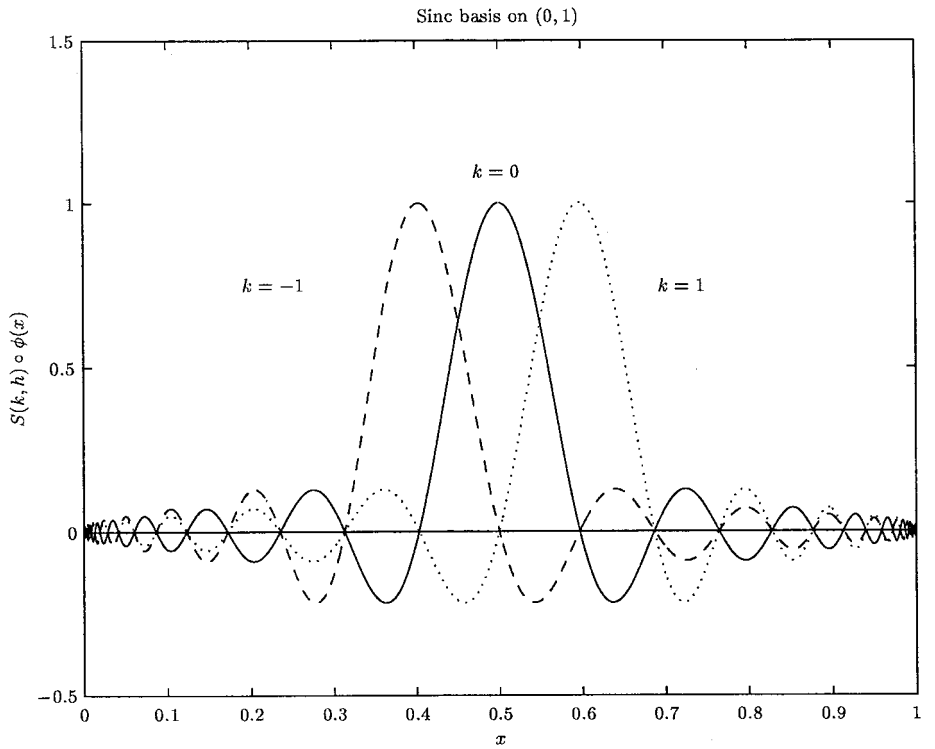

Figure A2. Three adjacent members ($S(k, h^*) \circ \phi(x)$, $k = -1, 0, 1$; $h^* = \pi/8$) of the mapped sinc basis on the interval (0, 1).

$$\delta^{(2)}_{jk} \equiv h^2 \frac{\mathrm{d}^2}{\mathrm{d}\phi^2}[S(j,h) \circ \phi(z)]\Big|_{z=z_k} = \begin{cases} \dfrac{-\pi^2}{3}, & k = j \\ \dfrac{-2(-1)^{k-j}}{(k-j)^2}, & k \neq j \end{cases} \tag{A.7}$$

These expressions are the elements of the Toeplitz matrices with the abbreviated notation $I^{(0)}$, $I^{(1)}$, and $I^{(2)}$. Note that if one were to write (more fully) $I^{(0)}_{k-j}$, $I^{(1)}_{k-j}$, and $I^{(2)}_{k-j}$ then

$$I^{(0)}_{k-j} = I^{(0)}_{j-k}, \qquad I^{(1)}_{k-j} = -I^{(1)}_{j-k}, \qquad I^{(2)}_{k-j} = I^{(2)}_{j-k}$$

since $I^{(0)}$ and $I^{(2)}$ are symmetric, while $I^{(1)}$ is skew-symmetric.

A.2. Sinc function approximations

The class of functions such that known exponential error estimates exist for infinite sinc interpolation and quadrature is denoted by $B(\mathscr{D}_{\mathrm{E}})$ and is defined next.

Definition A.1
Let $B(\mathscr{D}_E)$ be the class of functions F, which are analytic in $\mathscr{D}_E$, satisfy

$$\int_{\psi(t+L)} |F(z)\,dz| \to 0, \quad t \to \pm\infty$$

where $L = \{is: |s| < d \le \pi/2\}$, and on the boundary of $\mathscr{D}_E$ (denoted $\partial\mathscr{D}_E$) satisfy

$$\mathscr{N}(F) \equiv \int_{\partial\mathscr{D}_E} |F(z)\,dz| < \infty$$

Interpolation and quadrature (integration) rules for functions in $B(\mathscr{D}_E)$ are defined in the following theorems whose proofs are found in References [10,12]. These theorems are presented so as to be applicable to general conformal mapping functions $w = \phi(z)$ onto an interval of interest.

Theorem A.1
If $\phi' F \in B(\mathscr{D}_E)$ then for all $z \in \Gamma$,

$$F(z) = \sum_{j=-\infty}^{\infty} F(z_j) S(j,h) \circ \phi(z) + E_F \tag{A.8}$$

where

$$E_F \equiv \frac{\sin(\pi\phi(z)/h)}{2\pi i} \int_{\partial\mathscr{D}_E} \frac{\phi'(w)F(w)\,dw}{(\phi(w)-\phi(z))\sin(\pi\phi(w)/h)}$$

Theorem A.2
If $F \in B(\mathscr{D}_E)$ then

$$\int_\Gamma F(z)\,dz = h \sum_{j=-\infty}^{\infty} \frac{F(z_j)}{\phi'(z_j)} + I_F \tag{A.9}$$

where

$$I_F \equiv \frac{i}{2} \int_{\partial\mathscr{D}_E} \frac{F(z)\kappa(\phi,h)(z)}{\sin(\pi\phi(z)/h)}\,dz$$

with

$$\kappa(\phi, h)(z) = \exp\left[\frac{\mathrm{i}\pi\phi(z)}{h}\,\mathrm{sgn}(\mathrm{Im}(\phi(z)))\right]$$

For the Sinc–Galerkin method, the infinite quadrature rule must be truncated to a finite sum. The following theorem indicates the conditions under which exponential convergence results.

Theorem A.3
If $F \in B(\mathscr{D}_{\mathrm{E}})$ and there are positive constants α and C so that

$$\left|\frac{F(z)}{\phi'(z)}\right| \leq C \exp(-\alpha|\phi(z)|)$$

for all $z \in \Gamma$ then

$$\int_{\Gamma} F(z)\,\mathrm{d}z = h \sum_{j=-N}^{N} \frac{F(z_j)}{\phi'(z_j)} + \mathscr{O}(\exp(-\alpha N h)) + \mathscr{O}(\exp(-2\pi d/h)) \tag{A.10}$$

Hence, if $h = \sqrt{2\pi d/(\alpha N)}$, the exponential order of the sinc trapezoidal quadrature rule is $\mathscr{O}(\exp(-(2\pi d\alpha N)^{1/2}))$.

Corollary A.1
An important special case housed in (A.10) occurs when the integrand has the form $G(z)S(l, h) \circ \phi(z)$. Due to the interpolation $S(l, h) \circ \phi(z_j) = S(l, h)(jh) = \delta_{jl}^{(0)}$ (defined in (A.5)), the sinc quadrature rule is a weighted point evaluation to the order of the method

$$\int_{\Gamma} G(z)S(l, h) \circ \phi(z)\,\mathrm{d}z = h\,\frac{G(z_l)}{\phi'(z_l)} + \mathscr{O}(\exp(-2\pi d/h)) \tag{A.11}$$

For the reader more familiar with approximations derived using polynomial relationships, the error terms above may seem somewhat exotic; however, as seen in Theorems A.1 and A.2, the sinc approximations are derived using the residue theorem with contour integrals where the integrands are independent. This accounts for the error terms that are contour integrals with integrands containing the dependent variable, F, in contrast with error terms that involve higher-order derivatives of F. Given these error terms, the above expressions show sinc interpolation and quadrature on $B(\mathscr{D}_{\mathrm{E}})$ converge exponentially.

A.3. The general Sinc–Galerkin method

The orthogonalization of the residual in the Sinc–Galerkin method for a differential equation of the form

$$\mathscr{L}y = f \tag{A.12}$$

on Γ can be treated as follows. When y satisfies Dirichlet conditions at the end-points, one assumes an approximate solution y_m in the form of a series with $m = 2N + 1$ terms

$$y_m(z) = \sum_{j=-N}^{N} y_j S(j, h) \circ \phi(z) \tag{A.13}$$

The coefficients $\{y_j\}_{j=-N}^{N}$ are determined by orthogonalizing the residual $\mathscr{L}y_m - f$ with respect to the functions $\{S_k\}_{k=-N}^{N}$, which yields the discrete system

$$\int_{\Gamma} (\mathscr{L}y_m - f)(z) S(k, h) \circ \phi(z) \omega(z)\, \mathrm{d}z = 0 \tag{A.14}$$

for $-N \leq k \leq N$. The weight function $\omega(z)$ in the integrand is chosen depending on the boundary conditions, the domain and the differential equation.

The most direct development of the discrete system for (A.12) is obtained by substituting (A.13) into (A.14). This approach, however, obscures the analysis, which is necessary for applying sinc formulas to (A.14). An alternative approach is to integrate derivative terms in $\mathscr{L}y_m$ by parts to transfer derivatives from y_m to the sinc functions. The accurate approximation of the integrals in (A.14) is accomplished with the adroit application of the quadrature rules in Theorem A.3 and the sinc derivative expressions in (A.6) and (A.7). The resulting discrete system is the same as that arising from substitution of (A.13) into (A.14) to within the accuracy of the method.

APPENDIX B. QUADRATIC BOTTOM STRESS CONDITION

In References [6,7] three different seabed boundary conditions—linear and quadratic bottom stress and zero velocity, were examined. This appendix outlines how the quadratic bottom stress boundary condition can be incorporated into the Sinc–Galerkin method.

B.1. The bottom boundary condition

If a 'quadratic law of friction' is to be applied at the seabed, the bottom boundary conditions are then (compare with (2.3))

$$-\rho A_{\mathrm{v}}^{*}(D_0) \frac{\mathrm{d}\boldsymbol{q}^{*}(D_0)}{\mathrm{d}z^{*}} = \rho c_{\mathrm{d}} \boldsymbol{q}^{*}(D_0) \|\boldsymbol{q}^{*}(D_0)\|$$

where $\|\boldsymbol{q}^{*}(D_0)\|$ is the bottom current speed and c_{d} is a universal bottom drag coefficient. When (2.3) is non-dimensionalized, the condition at $z = 1$ can be expressed in component form as (compare with (2.6))

$$U(1) + \sigma_q \frac{\mathrm{d}U(1)}{\mathrm{d}z} = 0, \qquad V(1) + \sigma_q \frac{\mathrm{d}V(1)}{\mathrm{d}z} = 0$$

where

$$\sigma_q \equiv \frac{A_0 A_v(1)}{c_d D_0 \|\boldsymbol{q}(1)\|} \tag{B.1}$$

B.2. Modifications to the Sinc–Galerkin method

The efficiency and accuracy of the Sinc–Galerkin method makes feasible an iterative solution for $w(z) = u(z) + iv(z)$ with no special restrictions on the eddy viscosity. The iterative procedure is based on the Sinc–Galerkin solution of the system (2.12)–(2.16), with σ_q replacing σ and with $Q^{(1)}(1) < 1$ as a starting value for the speed $\|\boldsymbol{q}(1)\|$ in (B.1) to generate $\sigma_q^{(1)}$.

Improved values of the approximation to the speed, $Q(1)$, and hence improved values of the velocity $w(z)$ are computed by the solution of the Sinc–Galerkin system using $Q^{(1)}(1)$ and $\sigma_q^{(1)}$. This process continues, thus generating the sequences $Q^{(n)}(1)$ and $\sigma_q^{(n)}$. The iteration is terminated when $|Q^{(n+1)}(1) - Q^{(n)}(1)| < \epsilon$ for a prescribed tolerance ϵ.

In the case of Example 6.1, with $N = 8$, the error criterion assignment $\epsilon = 10^{-8}$ is satisfied at $n = 6$. Since only part of the code is involved in the iteration, the CPU time increases only by a factor of 2 over the linear case. The horizontal projections of the Ekman spirals corresponding to the quadratic stress and the linear stress bottom condition with $k_f = 0.002$ m s^{-1} are nearly the same, except over the bottom 20 m, where the near-bottom current speed is somewhat less for the linear bottom stress than that computed with a quadratic bottom stress. Although experiments similar to those in Example 5.1 demonstrate even smaller differences at all depths, in both cases a decrease in k_f by an order of magnitude provides agreement between the horizontal projections of the Ekman spirals over the entire water column.

REFERENCES

1. Ekman VW. On the influence of the earth rotation on ocean currents. *Royal Swedish Academy of Science*, *Arkiv foer matematik*, *astronomi och fysik* 1905; **2**(11): 1–53.
2. Defant A. *Physical Oceanography*, vol. 1. Pergamon Press: Oxford, 1961.
3. Heaps NS. On the numerical solution of the three-dimensional hydrodynamical equations for tides and storm surges. *Memoirs of the Society of Science*, *Liege*, *Series 6* 1971; **1**: 143–180.
4. Heaps NS. Development of a three-dimensional numerical model of the Irish Sea. *Rapp Rev Reun Cons Int Explor Mer*, *Sec 3; Models* 1974; **167**: 147–162.
5. Heaps NS. Three-dimensional model for tides and surges with vertical eddy viscosity prescribed in two layers: I. Mathematical formulation. *Geophysical Journal of the Royal Astronomical Society* 1981; **64**: 291–302.
6. Davies AM. The numerical solution of the three-dimensional hydrodynamical equations using a B-spline representation of the vertical current profile. In *Bottom Turbulence*, Nihoul JCJ (ed.). Elsevier: New York, 1977; 1–25.
7. Davies AM, Owen A. Three-dimensional numerical sea model using Galerkin method with a polynomial basis set. *Applied Mathematical Modelling* 1979; **3**: 421–428.
8. Davies AM. Spectral models in continental shelf oceanography. In *Three-Dimensional Coastal Ocean Models*, Heaps NS (ed.). American Geophysical Union: Washington, DC, 1987; 77–106.
9. Bowers KL, Carlson TS, Lund J. Advection–diffusion equations: Temporal sinc methods. *Numerical Methods for Partial Differential Equations* 1995; **11**(4): 399–422.
10. Lund J, Bowers KL. *Sinc Methods for Quadrature and Differential Equations*. SIAM: Philadelphia, PA, 1992.
11. Stenger F. Numerical methods based on Whittaker cardinal, or sinc functions. *SIAM Review* 1981; **23**(2): 165–224.

12. Stenger F. *Numerical Methods Based on Sinc and Analytic Functions*. Springer: New York, 1993.
13. Davies AM, Luyten PJ, Deleersnijder E. Turbulence energy models in shallow sea oceanography. In *Quantitative Skill Assessment for Coastal Ocean Models*, *Coastal and Estuarine Studies*, vol. 47, Lynch DR, Davies AM (eds). American Geophysical Union: Washington, DC, 1995; 97–123.
14. Naimie CE. A turbulent boundary layer model for the linearized shallow water equations, NUBBLE USER'S MANUAL (Release 1.1). Technical Report NML-96-1, Dartmouth College, 31 July, 1996.
15. Large WG, Pond S. Open ocean momentum flux measurements in moderate to strong winds. *Journal of Physical Oceanography* 1981; **11**: 324–336.

